

The inverse parametric problem

Michele Cortinovis, Fabio Lingua,* and David B. Haviland

Department of Applied Physics, KTH Royal Institute of Technology, SE-10691 Stockholm, Sweden

(Dated: December 18, 2025)

We present a method to calculate the frequency components of a pump waveform driving a parametric oscillator, which realizes a desired frequency mixing or scattering between modes. The method is validated by numerical analysis and we study its sensitivity to added Gaussian noise. A series of experiments apply the method and demonstrate its ability to realize complex scattering processes involving many modes at microwave frequencies, including non-reciprocal mode circulation. We also present an approximate method to dynamically control mode scattering, capable of rapidly routing signals between modes in a prescribed manner. These methods are useful tools for encoding and manipulating continuous variable quantum information with multi-modal Gaussian states.

I. INTRODUCTION

Parametric oscillators are a universal paradigm for a variety of applications across physics. They are extensively used in quantum technologies for quantum limited amplification [1], coupling qubits [2], quadrature squeezing [3–10], as well as engineering entanglement through frequency mixing and second-harmonic generation, at microwave [11–17], and at optical wavelengths [18–20].

A parameter of an oscillator is externally controlled by a coherent drive known as the *pump*. The pump can be a continuous wave consisting of a single frequency, or a periodic waveform consisting of a sum of multiple tones. The frequency, amplitude, and phase of these tones define the pump waveform, effectively controlling the parametric process. Given a particular pump waveform $p_L(t)$, a direct computation of the equation-of-motion matrix \mathbf{M} yields the scattering matrix \mathbf{S} which describes how an input $a_{\text{in}}(t)$ is transformed to an output $a_{\text{out}}(t)$ (see fig. 1a) [21, 22]. We call this computation the *direct parametric problem* (see fig. 1c), useful for describing parametric amplification [23], entanglement generation [11–15], multi-mode squeezing and cluster state generation [16, 17, 19, 20], signal routing and frequency conversion [22, 24, 25], even non-reciprocal [26, 27].

More interesting in many applications is a solution to the *inverse parametric problem*: given a desired scattering matrix, what is the required pump waveform? Previous attempts to solve this problem have relied on optimization methods such as automated pump shaping [28], discovery of coupled-mode networks [29], or machine learning strategies [30]. To our knowledge, a general and systematic framework for solving the inverse parametric problem has remained an open challenge.

Here we propose an exact solution to this problem. The method relies on mode-coupling theory [22] where each pump frequency is an element of an orthogonal basis spanning the Hilbert space of all possible matrices \mathbf{M} . Defining a suitably normalized inner product

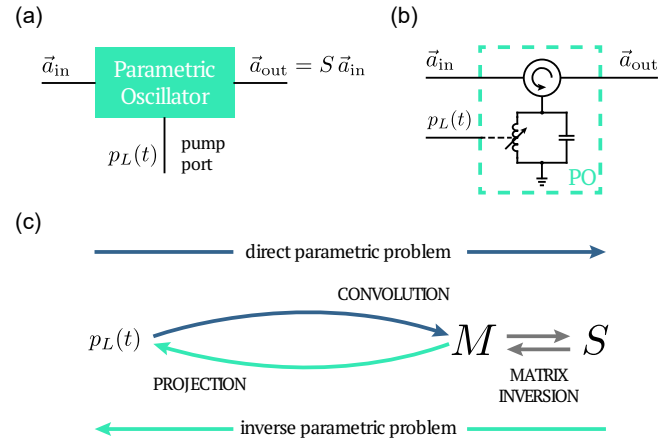


FIG. 1. (a) General I/O relation of a parametric oscillator where the output is determined by the scattering matrix \mathbf{S} , controlled by the pump $p_L(t)$. (b) Example of a parametric oscillator, the pump port modulates the inductance of an LC oscillator. (c) We define direct problem when the knowledge of $p_L(T)$ allows to compute the scattering matrix \mathbf{S} , inverse problem when from a target \mathbf{S} one recover the pump signal that realizes it.

on this Hilbert space, we directly obtain the amplitude and phase at each pump frequency as a projection of the \mathbf{M} that gives the desired output. We implement the method numerically and assess its robustness against noise, demonstrating the ability to reconstruct randomly generated scattering matrices. We use the method to design a multi-port device described by a given ideal target scattering matrix. We also demonstrate another method which encodes arbitrary information in the output modes by dynamically changing the pump waveform.

* lingua@kth.se

II. PARAMETRIC OSCILLATOR AND INVERSE PROBLEM

A general parametric oscillator is described by the time-dependent Hamiltonian

$$\hat{\mathcal{H}}_{\text{PO}} = \frac{\omega_0}{2} (A^\dagger A + A A^\dagger) + \frac{\omega_0}{2} p_L(t) (A + A^\dagger)^2, \quad (1)$$

where A and A^\dagger are the annihilation and creation operators of the oscillator mode with resonant frequency ω_0 , which is modulated by a pump $p_L(t)$. We consider pump waveforms that are periodic over a time interval T , expressed as a coherent superposition of tones with frequencies Ω_k , amplitudes p_k , and phases ϕ_k :

$$p_L(t) = \sum_k p_k \cos(\Omega_k t + \phi_k) = \sum_k (g_k e^{-i\Omega_k t} + g_k^* e^{i\Omega_k t}), \quad (2)$$

where $g_k = \frac{p_k}{2} e^{i\phi_k}$ are the complex pump amplitudes.

The parametric oscillator is coupled to an external bath of modes, allowing an input–output description of its dynamics. In superconducting implementations, this coupling typically occurs through input and output transmission lines, as illustrated in Fig. 1(b). The oscillator mode A (A^\dagger) is coupled to the continuum of propagating modes in the transmission lines, described by the field operators $a(\omega)$ and $a^\dagger(\omega)$. The finite measurement time T sets the frequency resolution $\Delta = 1/T$, so that the field in the transmission line is represented by a discrete set of orthogonal frequency modes a_m and a_m^\dagger . A convenient way to model the dynamics of the parametric oscillator is to expand Eq. (1) in the frequency-mode basis of the transmission lines, $A^{(\dagger)} = \sum_m a_m^{(\dagger)} e^{-i\omega_m t}$ (see Ref. [25] for a detailed derivation).

This expansion transforms the time-dependent Hamiltonian into a time-independent system of N coupled harmonic oscillators [22, 24, 25]. The resulting equation of motion (EOM) for the m^{th} mode in the frequency domain reads

$$i(\omega_m + \tilde{\omega}_0) a_m + i \sum_n (g_{mn} a_n + g_{mn}^* a_n^\dagger) = \sqrt{\gamma} a_{\text{in},m}, \quad (3)$$

where $\tilde{\omega}_0 = \omega_0 - i\gamma/2$ and γ denotes the coupling rate to the transmission line, assumed constant for all modes.

The parametric pump enables intermodulation, or frequency mixing between modes through the couplings $g_{mn} = \sum_k g_k \delta_{m,n \pm k}$, which connect modes satisfying the condition $\omega_m \pm \omega_n = \pm \Omega_k$. This mixing is a direct consequence of multiplication with $p_L(t)$ in Eq. 1, which is a convolution in the frequency domain (see [25] for further details).

The equations of motion can be compactly written in matrix form as

$$-i\gamma \mathbf{M} \vec{a} = \sqrt{\gamma} \vec{a}_{\text{in}}, \quad (4)$$

where $\vec{a} = (a_1, a_1^\dagger, \dots, a_N, a_N^\dagger)^T$ collects all mode operators satisfying the bosonic commutation relations

$[a_m, a_n^\dagger] = \delta_{mn}$. In the classical limit $a_m^{(\dagger)} \rightarrow a_m^{(*)} \in \mathbb{C}$. Following Ref. [24], we normalize \mathbf{M} by γ .

We distinguish two types of pumps, low frequency (LF, sometimes called beam-splitter or frequency conversion) pumps $\Omega_k = k\Delta \ll \omega_0$ with $k \in \mathbb{N}$, and high frequency (HF, sometimes called squeezing) pumps $\Omega_{k'} = 2\omega_0 + k'\Delta$ with $k' \in \mathbb{Z}$, and we decompose the $2N \times 2N$ matrix \mathbf{M} to a general form,

$$\mathbf{M} = \mathbf{M}_d + \sum_k \mathbf{L}_k + \sum_{k'} \mathbf{H}_{k'}, \quad (5)$$

Here \mathbf{M}_d is diagonal with elements $\Delta_m = \frac{1}{\gamma}(-\omega_m - \tilde{\omega}_0) \in \mathbb{C}$, and \mathbf{L}_k and $\mathbf{H}_{k'}$ are the coupling matrices associated with the low- and high-frequency pumps, respectively.

The matrices \mathbf{L}_k exhibit two off-diagonals at $\pm 2k$,

$$\mathbf{L}_k = \begin{pmatrix} 0 & l_k & & & \\ 0 & -l_k^* & & & \\ \ddots & \ddots & \ddots & & \\ l_k^* & 0 & l_k & & \\ -l_k & 0 & -l_k^* & & \\ \ddots & \ddots & \ddots & \ddots & \\ l_k^* & 0 & -l_k & 0 & \\ -l_k & 0 & 0 & l_k & \end{pmatrix}, \quad (6)$$

while the matrices $\mathbf{H}_{k'}$ contain a single anti-diagonal at $2k'$

$$\mathbf{H}_{k'} = \begin{pmatrix} 0 & & & h_{k'} & \\ 0 & -h_{k'}^* & & & \\ \ddots & \ddots & \ddots & & \\ \ddots & \ddots & \ddots & 0 & \\ h_{k'} & 0 & & 0 & \\ -h_{k'}^* & 0 & & & \ddots \\ & & & & 0 \end{pmatrix}. \quad (7)$$

For clarity, we distinguish between $l_k = \frac{g_k}{\gamma}$ and $h_{k'} = \frac{g_{k'}}{\gamma}$, which are the normalized complex pump amplitudes of the low- and high-frequency pumps, respectively. There are $N_{LF} = N - 1$ low frequency pumps and $N_{HF} = 2N - 1$ high-frequency pumps. Thus, in total there are $N_{\text{tot}} = N_{LF} + N_{HF} = 3N - 2$ pumps.

The solution of (4) is readily available upon matrix inversion, $\vec{a} = \frac{i}{\sqrt{\gamma}} \mathbf{M}^{-1} \vec{a}_{\text{in}}$. The scattering matrix of input–output theory is then derived from the mode matching condition $\sqrt{\gamma} \vec{a} = \vec{a}_{\text{in}} + \vec{a}_{\text{out}}$,

$$\mathbf{S} = i\mathbf{M}^{-1} - \mathbb{1}. \quad (8)$$

In summary, frequency-domain knowledge of the periodic pump allows for discrete convolution leading to \mathbf{M} in (4), which upon inversion yields \mathbf{S} in (8). Note that \mathbf{S} in the a_i, a_i^* basis is a $2N \times 2N$ complex matrix, with

elements $S_{mn} = |S_{mn}|e^{i\phi_{mn}}$ defined by magnitude and phase, both determined by the combined action of the pumps. This formally defines the direct problem illustrated in Fig. 1(c). The inverse parametric problem is the computation of the pump waveform necessary to realize a given target scattering matrix \mathbf{S}_\odot . Its solution requires de-convolution, which is generally not trivial.

A. Solving the inverse problem

In the decomposition of \mathbf{M} in (5), the pump-induced coupling matrices \mathbf{L}_k , and $\mathbf{H}_{k'}$ exhibit internal symmetries, reflecting the identical action of each pump tone across all frequency modes. These symmetries allow us to further decompose the coupling matrices as

$$\mathbf{L}_k = l_k \mathbf{L}_k^+ + l_k^* \mathbf{L}_k^-, \quad \mathbf{H}_{k'} = h_{k'} \mathbf{H}_{k'}^+ + h_{k'}^* \mathbf{H}_{k'}^-, \quad (9)$$

where the $l_k, h_{k'} \in \mathbb{C}$ are normalized complex pump amplitudes, and the matrices \mathbf{L}_k^\pm and $\mathbf{H}_{k'}^\pm$, which have only elements ± 1 and 0, are defined in Appendix A.

To determine the complex pump amplitudes l_k and $h_{k'}$ we introduce the Frobenius (Hilbert–Schmidt) inner product between two matrices,

$$(\mathbf{A}, \mathbf{B}) = \text{Tr}(\mathbf{A} \cdot \mathbf{B}^T), \quad (10)$$

With respect to this inner product the set of all \mathbf{L}_k^\pm and $\mathbf{H}_{k'}^\pm$ form a orthogonal basis in the space of complex $2N \times 2N$ matrices:

$$\begin{aligned} (\mathbf{L}_k^\pm, \mathbf{L}_q^\pm) &= 2(N - k) \delta_{kq}, \\ (\mathbf{H}_{k'}^\pm, \mathbf{H}_{q'}^\pm) &= (N - |k'|) \delta_{k'q'}, \\ (\mathbf{L}_k^\pm, \mathbf{H}_{q'}^\pm) &= 0. \end{aligned} \quad (11)$$

We define the off-diagonal components of \mathbf{M} as $\Delta\mathbf{M} \equiv \mathbf{M} - \mathbf{M}_d$, which collects all pump-induced mode couplings. Eq. (5) together with Eq. (9), and the orthogonality relations (11), imply that we can expand $\Delta\mathbf{M}$ as

$$\Delta\mathbf{M} = \sum_k (l_k \mathbf{L}_k^+ + l_k^* \mathbf{L}_k^-) + \sum_{k'} (h_{k'} \mathbf{H}_{k'}^+ + h_{k'}^* \mathbf{H}_{k'}^-). \quad (12)$$

Thus the matrices $\{\mathbf{L}_k^\pm, \mathbf{H}_{k'}^\pm\}$ constitute an orthogonal basis spanning the Hilbert space that contains all possible coupling matrices $\Delta\mathbf{M}$. In this framework, the complex pump amplitudes are expansion coefficients, obtained by projecting $\Delta\mathbf{M}$ onto the corresponding basis elements:

$$l_k^{(*)} = \frac{(\Delta\mathbf{M}, \mathbf{L}_k^\pm)}{\|\mathbf{L}_k^\pm\|}, \quad h_{k'}^{(*)} = \frac{(\Delta\mathbf{M}, \mathbf{H}_{k'}^\pm)}{\|\mathbf{H}_{k'}^\pm\|}, \quad (13)$$

where $\|\mathbf{A}\| = \sqrt{(\mathbf{A}, \mathbf{A})}$ denotes the Frobenius norm.

In summary, given a target scattering matrix \mathbf{S}_\odot , Eq. (8) is inverted to yield the corresponding target

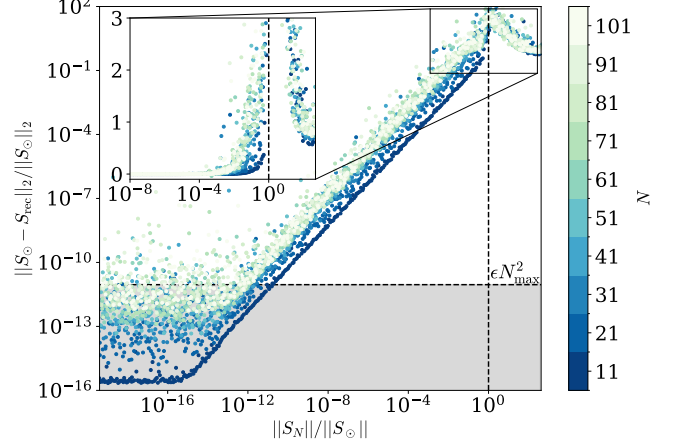


FIG. 2. Robustness of the PPM against Gaussian noise. Relative reconstruction error $\|\mathbf{S}_\odot - \mathbf{S}_{\text{rec}}\|_2 / \|\mathbf{S}_\odot\|_2$ as a function of the noise-to-target ratio $\|\mathbf{S}_N\|_2 / \|\mathbf{S}_\odot\|_2$ for different matrix sizes $2N$. The horizontal dotted line indicates the numerical-precision for the maximum number of modes tested N_{max} . The vertical dotted line marks unity noise-to-target ratio, beyond which the PPM becomes unreliable.

equation-of-motion matrix \mathbf{M}_\odot , and its off-diagonal components $\Delta\mathbf{M}_\odot$:

$$\Delta\mathbf{M}_\odot = -i(\mathbf{S}_\odot + \mathbb{1})^{-1} - \mathbf{M}_\odot d. \quad (14)$$

Substituting $\Delta\mathbf{M}_\odot$ into Eqs. (13) provides the complete set of complex coefficients $\{l_k, h_{k'}\}$, directly yielding the amplitude and phase of each pump tone. This method, which we refer to as the *Pump Projection Method* (PPM), constitutes an exact and closed-form solution to the inverse parametric problem.

B. Testing the Pump Projection Method

We validate the PPM through numerical simulations on a set of 10^4 randomly generated target scattering matrices of different sizes $2N$. Each target matrix \mathbf{S}_\odot is produced by solving the direct problem for a randomly generated pump waveform consisting of $3N - 2$ tones, both low and high frequency pumps with random amplitude and phase (see appendix A). Solving the inverse problem for \mathbf{S}_\odot yields the corresponding pump waveform, which we use in the direct problem to reconstruct a scattering matrix \mathbf{S}_{rec} . The deviation between \mathbf{S}_\odot and \mathbf{S}_{rec} benchmarks the accuracy of the method. Up to numerical precision, our implementation of the PPM is always able to recover the original pump waveform.

To assess robustness, Gaussian noise of variable magnitude is added to the target matrix \mathbf{S}_\odot . We quantify the error in the PPM as the relative deviation from the noise-free target $\|\mathbf{S}_\odot - \mathbf{S}_{\text{rec}}\|_2 / \|\mathbf{S}_\odot\|_2$ where $\|\cdot\|_2$ denotes the matrix 2-norm. In Fig. 2 we plot this relative deviation as a function of the noise-to-target ratio $\|\mathbf{S}_N\|_2 / \|\mathbf{S}_\odot\|_2$. We

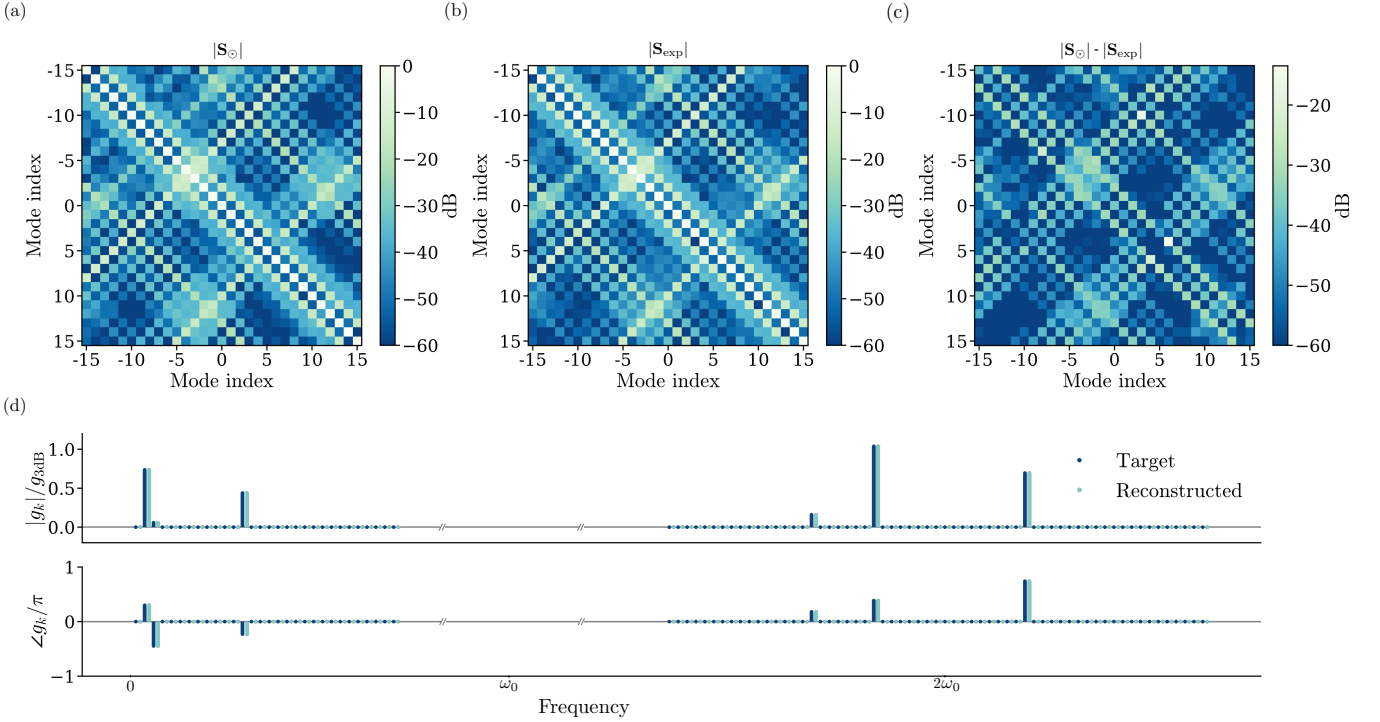


FIG. 3. Experimental validation of the Pump Projection Method (PPM). (a) Target scattering matrix S_0 constructed from the target pumps (blue) shown in (d). (b) Experimentally measured scattering matrix S_{exp} obtained from the reconstructed pumps (cyan) shown in (d). (c) Difference between the magnitudes of the target and measured scattering matrices. (d) Pump amplitude (upper) and phase (lower). Amplitudes are normalized by the single-frequency pump amplitude at $2\omega_0$, which achieves 3dB gain in the JPA.

averaged over 100 noise configurations and repeated the study for different numbers of modes N , corresponding to different matrix sizes. As shown in Fig. 2, the error scales linearly with the noise magnitude and remains bounded from below by numerical precision ϵ . The grey shaded area marks the region dominated by numerical noise ϵN^2 , for the largest matrix size $2N_{\text{max}}$. The inset illustrates the divergence of the error as the noise-to-target ratio approaches unity, indicating that the method breaks down. Thus, the PPM gives a faithful reconstruction of the pump waveform, even in the presence of significant noise, across all matrix sizes.

In addition to numerical tests, we verify the performance of the PPM with an experiment on a Josephson Parametric Amplifier (JPA) in a setup described in Appendix B. Figure 3 shows a representative example in which the PPM reconstructs the pump waveform for a given target scattering matrix. Panel 3(a) displays the target matrix S_0 obtained from a randomly generated pump waveform, and panel 3(b) shows the experimentally measured matrix S_{exp} obtained from the reconstructed pump waveform. Here, the mode index 0 corresponds to the resonant frequency of the JPA. The two matrices exhibit excellent agreement as shown in Figure 3(c), with a total relative deviation of $\|S_0 - S_{\text{exp}}\|_2/\|S_0\|_2 = 0.037$; the residual discrepancy is primarily set by the experimental background noise

floor in Fig. 3(b). Panel 3(d) shows the corresponding pump waveforms, illustrating the distribution of amplitudes and phases for the target pump tones (blue) and reconstructed (cyan). These results validate the PPM beyond numerical simulation, demonstrating its application in an experiment.

C. Applications

The PPM is very effective at recovering the pumping scheme when one has full knowledge of both magnitude and phase of the elements of the target scattering matrix. When designing a target scattering matrix for a practical application, e.g. a signal routing between frequency modes, we often consider only magnitudes, which define how power is distributed between modes. The associated phases may be unknown, yet they may play an important role in the redistribution of power. For a given set of target magnitudes, only specific phase configurations correspond to physically realizable scattering matrices. The PPM projects onto a pump configuration which generates a closely associated, but realizable scattering matrix. Consequently, if the phases of the target are inconsistent with the desired magnitudes, the recovered pumping scheme generates scattering which may deviate significantly from the target.

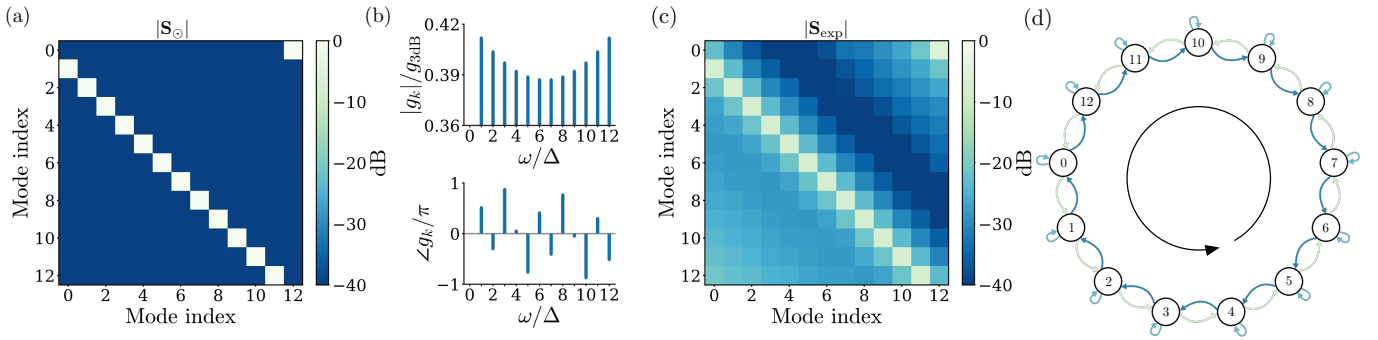


FIG. 4. Design and implementation of a 13-mode circulator using the PPM. (a) Target scattering matrix $|\mathbf{S}_0|$ designed in the xp basis. (b) Low frequency pump amplitudes (top) and phases (bottom) of the waveform returned by the PPM. (c) Experimentally measured scattering matrix $|\mathbf{S}_{\text{exp}}|$, obtained by applying the pump waveform from panel (b). (d) Graphical representation of the 13-mode circulator. Black arrow shows the circulation direction.

We know of no universal or optimal strategy to compensate for lack of knowledge of the phases. We have identified several practical guidelines for constructing a target \mathbf{S}_0 . (i) It is often easier to start in the (x_i, p_i) basis with $\mathbf{S}_0 = U \mathbf{S}_0 U^\dagger$, where U is the canonical transformation from (a_i, a_i^\dagger) to (x_i, p_i) . In the (x_i, p_i) basis we can apply the constraint that \mathbf{S}_0 must be both real and symplectic, automatically enforcing the correct phase relations between creation and annihilation operators. (ii) Symmetry considerations, e.g. non-reciprocity, can serve as valuable criteria for guiding the design. (iii) An iterative workflow, where the target scattering matrix is progressively refined. A new target is constructed by altering a calculated scattering matrix using pumps returned by the PPM in the previous iteration.

With these guidelines we use the PPM to obtain the pump waveform that realizes a 13-mode circulator, as shown in Fig. 4. The nonreciprocal target scattering matrix of an ideal 13-mode circulator shown in Fig. 4(a). This scattering matrix is not physically realizable for arbitrary magnitude of the off diagonal elements. Following the principles discussed above we use the PPM to iterate through the magnitude of the off-diagonal elements of \mathbf{S}_0 , maximizing for nonreciprocity of the recovered scattering matrix, $\max [|\mathbf{S}_{\text{rec}}| - |\mathbf{S}_{\text{rec}}^T|]$. We arrive at the pumping scheme shown in Fig. 4(b) which contains only LF pumps. Programming this pumping scheme into our multifrequency lock in amplifier, we generate the measured scattering matrix shown in Fig. 4(c). Panel 4(d) illustrates the resulting circular routing between the 13 frequency modes, where the color coded arrows depict the magnitude of the dominant scattering processes. We do not achieve ideal circulation, but the unwanted scattering channels are suppressed by more than -20 dB, with approximately -6 dB transmission between modes in the desired direction of circulation.

D. Dynamic control of Scattering

The PPM is useful for determining pumping schemes to realize complicated scattering matrices, but it can be slow in finding a satisfactory result, especially when the phases are unknown. Here we demonstrate an alternative method to quickly calculate a pumping scheme which approximates the desired scattering, when only the magnitude is known. We can rapidly reprogram the pumps in an experiment where the pump waveform is updated every $T_{\text{col}} = 50$ ms. Each pump configuration is designed to generate a matrix \mathbf{S}_ℓ which scatters a single input tone into a desired set of output tones that code the pixel intensities of the ℓ^{th} column of an image. To a good approximation the pump waveform that realizes each \mathbf{S}_ℓ is composed of N_p HF pumps at the frequencies $\Omega_k = 2\omega_0 + k\Delta$ where $k \in [-N_p, 0]$, with amplitude $|h_k| \propto \text{Pix}_{k\ell}$, and with random phase $\phi_k = \text{rand}[0, 2\pi]$. The choice of random phase facilitates average cancellation of the higher order mixing processes through destructive interference, allowing the second-order intermodulation products generated by the HF pumps to dominantly contribute to the target \mathbf{S}_ℓ .

We performed an experiment encoding an image which is reproduced in Fig. 5(a). An example scattering matrix \mathbf{S}_ℓ used to reproduce the column of pixels at $t_\ell/T = 40$ (white dashed line) is shown in 5(b). During each time window starting at $t_\ell = \ell T_{\text{col}}$, $\ell \in [1, N_p]$: (i) a weak coherent tone is continuously applied at a fixed input frequency ω_{-45} (green arrow in Fig. 5(a)); (ii) the pump waveform corresponding to the ℓ -th image column is applied to the flux port of the JPA; and (iii) the full set of output frequency modes is simultaneously measured using the multifrequency lock-in amplifier.

Figure 5 shows the measured amplitudes of the output modes as a function of normalized time t/T_{col} . The scattered output evolves dynamically over the sequence, accurately reproducing the image encoded in the time series of pump waveforms. The amplitudes are expressed in decibels and normalized to the pump-off reference case.

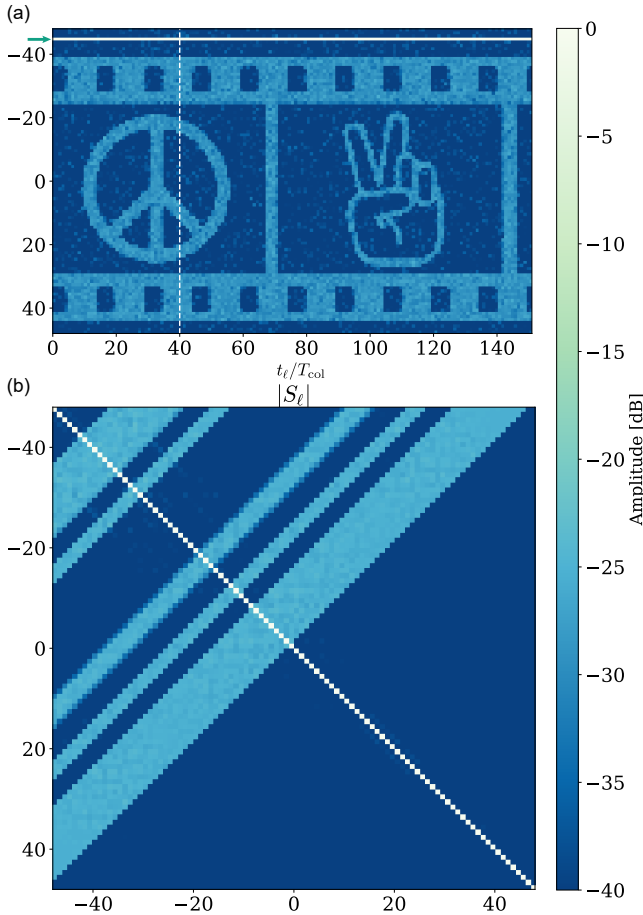


FIG. 5. (a) Measured output mode amplitudes as a function of time t_e/T . The pump waveform is dynamically updated every measurement window T , encoding successive columns of the target image. The scattered output evolves in time to reproduce the desired pattern, with amplitudes expressed in decibels and normalized to the pump-off reference. (b) Example of target scattering matrix S_e used to generate the output at $t_e/T = 40$ (white dashed line in panel (a)).

The high contrast in the image generated by rapidly changing the scattering of a single tone, highlights the ability to realize arbitrary, time-dependent transformations of the scattering matrix. See Appendix B for implementation details.

III. CONCLUSION

We introduced the Pump Projection Method (PPM), a general and closed-form solution to the inverse parametric problem for a single pole parametric circuit. By projecting the off-diagonal structure of the equation-of-motion matrix onto an orthogonal basis, the PPM directly returns the complete set of pump amplitudes and phases required to realize a desired scattering matrix. We validated the method numerically and studied its sensitivity to the addition of controlled Gaussian noise.

The reconstruction error scales linearly with the noise amplitude and remains bounded by numerical precision, demonstrating robustness of the method.

We tested the method in experiments with a Josephson Parametric Amplifier (JPA) thermalized at 10 mK. With a randomly generated target scattering matrix, we showed that the method recovers a pump waveform that, when applied to the JPA, realizes a measured scattering matrix with a relative deviation to the target of 3.7%. We used the PPM to engineer circulation between 13 frequency modes in the JPA, with more than -20 dB attenuation of scattering to unwanted channels, and transmission of -6 dB in the desired direction. These results demonstrate that the PPM is a practical method which reliably enables the design and implementation of complex scattering that is extremely challenging to obtain by intuition alone. We further introduce an approximate method for designing a pump that is capable of rapidly reconfiguring scattering, to dynamically encode arbitrary information in the output modes.

An interesting extension of the PPM is the exploration of frequency-mode coupling by parametrically modulating circuits with multiple poles. For example a parametric band-pass filter which sharply defines region of the spectrum where frequency modes scatter in to one-another. The ability to engineer the scattering matrix is of particular importance for continuous-variable quantum information [31] where the primary resources are Gaussian states which are fully specified by their first and second moments. When vacuum is injected into the pumped parametric oscillator, the output covariance matrix \mathbf{V} is entirely determined by the scattering matrix via

$$\mathbf{V} = \frac{\hbar}{2} \mathbf{S} \mathbf{S}^T. \quad (15)$$

This relation implies that the design of an arbitrary Gaussian state is equivalent to the design of its scattering matrix. The PPM therefore provides a direct way to compute the pump waveform and realize a desired covariance matrix. Its application with a multifrequency lockin amplifier makes for easy experimental realization of very complex mode couplings, opening up new opportunities for Gaussian-state engineering and multi-modal quantum technologies.

ACKNOWLEDGMENTS

We acknowledge Joe Aumentado at the National Institute of Standards and Technology (NIST) for helpful discussions and for providing the JPA used in this experiment. This work was partially supported by the Knut and Alice Wallenberg Foundation through the Wallenberg Center for Quantum Technology (WACQT), the Swedish Natural Science Research Council (VR) and the Olle Engkvist foundation.

AUTHOR DECLARATION

F. L. derived the theoretical method, M. C. implemented it numerically. F. L. and M. C. performed the numerical benchmarking and validating experiments. D. B. H. supervised the work. All authors edited, discussed and reviewed the manuscript.

D. B. H. is part owner of the company Intermodulation Products AB, which produces the digital microwave platform used in this experiment.

DATA AVAILABILITY

The data that support the findings of this study are openly available in Zenodo at [\[\]](#).

Appendix A: The coupling matrices

The pump coupling matrices (6) and (7) contain the collective action of each pump tone on the different frequency modes. Their structure is revealed by extracting the constants l_k , l_k^* and $h_{k'}$, $h_{k'}^*$.

$$\mathbf{L}_k = l_k \mathbf{L}_k^+ + l_k^* \mathbf{L}_k^-, \quad (A1)$$

$$\mathbf{H}_{k'} = h_{k'} \mathbf{H}_{k'}^+ + h_{k'}^* \mathbf{H}_{k'}^-, \quad (A2)$$

\mathbf{L}_k^\pm , and $\mathbf{H}_{k'}^\pm$ are constant, $2N \times 2N$ matrices of the form:

$$\mathbf{L}_k^+ = \begin{pmatrix} 0 & 1 & & & \\ 0 & 0 & 0 & & \\ \ddots & \ddots & \ddots & & \\ 0 & 0 & 0 & 1 & \\ -1 & 0 & 0 & 0 & 0 \\ \ddots & \ddots & \ddots & & \\ 0 & 0 & 0 & & \\ & -1 & 0 & & \\ & & 0 & & \\ & & & -1 & 0 \\ & & & & 0 \end{pmatrix}, \quad (A3)$$

$$\mathbf{L}_k^- = \begin{pmatrix} 0 & 0 & & & \\ 0 & 0 & -1 & & \\ \ddots & \ddots & \ddots & & \\ 1 & 0 & 0 & 0 & \\ 0 & 0 & 0 & -1 & \\ \ddots & \ddots & \ddots & & \\ 1 & 0 & 0 & & \\ & 0 & 0 & & \\ & & 0 & & \end{pmatrix}, \quad (A4)$$

$$\mathbf{H}_{k'}^+ = \begin{pmatrix} 0 & & & 1 & \\ 0 & 0 & & 0 & \\ \ddots & \ddots & \ddots & & \\ 1 & \ddots & \ddots & 0 & \\ 0 & & & 0 & \ddots \\ & & & & 0 \end{pmatrix}, \quad (A5)$$

$$\mathbf{H}_{k'}^- = \begin{pmatrix} 0 & & & 0 & \\ 0 & 0 & & -1 & \\ \ddots & \ddots & \ddots & & \\ 0 & \ddots & \ddots & 0 & \\ -1 & & & 0 & \ddots \\ & & & & 0 \end{pmatrix}. \quad (A6)$$

Appendix B: Experimental setup

Figure 6 shows a schematic of the experimental setup. The experiments are performed in a dilution refrigerator (Bluefors LD250) at millikelvin temperature. The parametric oscillator is Josephson Parametric Amplifier (JPA) designed for broad-band (100 MHz) gain, with loaded quality factor of about $Q = 37.5$. The JPA resonance is tuned by magnetic flux threading a SQUID loop. The DC flux adjusts the operating point (resonance frequency) and the AC flux is externally controlled by the pump waveform. DC bias and low-frequency pumps are combined with high frequency pumps using a cryogenic bias-tee. The input and output share the same signal port and they are separated close to the JPA by a cryogenic circulator. The reflected signal passes through two isolators before reaching a low-noise HEMT amplifier at 4 K. Attenuation and filtering are distributed along the signal line to thermalize the incoming radiation and suppress noise from higher temperature stages.

A typical experiment uses a DC flux close to half a flux quantum, where the resonance frequency is approximately 4.2 GHz. The pumps modulates the SQUID inductance, generating frequency mixing among the modes connected to the signal port. All pump and probe tones are synthesized and detected by a digital multi-frequency lock-in amplifier (PRESTO, Intermodulation Products AB). The instrument performs coherent modulation and demodulation at up to 192 frequencies simultaneously (i.e. in the same time window) with one reference phase for all frequencies, and digital control of the amplitude and phase of both signal and pump. The second Nyquist zone of the digital-to-analog converters is used to generate microwave signals from 3 to 10 GHz. Under-sampling

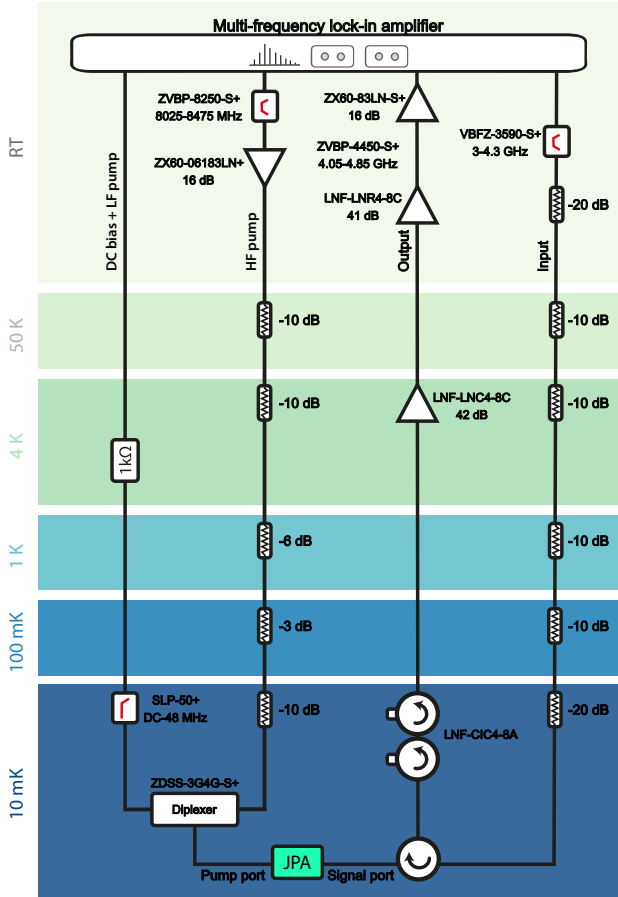


FIG. 6. Experimental setup used in this paper with a Josephson Parametric Amplifier used as the parametric oscillator.

and aliasing are used to down-convert the measured signals to the first Nyquist zone of the analog-to-digital converters. Analog filters at room temperature select the desired Nyquist zones for both up- and down-conversion. With this approach, digital multipliers replace the analog IQ mixers traditionally used at microwave frequencies. This all-digital approach enables phase coherence between all frequency components, essentially defining the orthonormal comb of modes in the measurement time window T , and the corresponding frequency spacing of the modes $\Delta = 1/T$. All frequencies in the comb and the digital sampling clock are related by a rational fraction, establishing a frequency-comb basis, ensuring orthogonality of the modes and eliminating Fourier leakage between them. In the measurements presented here, the spacing was set to $\Delta = 100$ kHz, much smaller than the linewidth of the JPA ~ 100 MHz, so that all modes of the comb are well within the amplifier bandwidth. Scattering measurements typically average over 5×10^3 windows T .

- [1] Carlton M. Caves, Joshua Combes, Zhang Jiang, and Shashank Pandey. Quantum limits on phase-preserving linear amplifiers. *Physical Review A*, 86(6):063802, December 2012.
- [2] P. Bertet. Parametric coupling for superconducting qubits. *Physical Review B*, 73(6), 2006.
- [3] B. Yurke. Squeezed-state generation using a Josephson parametric amplifier. *JOSA B*, Vol. 4, Issue 10, pp. 1551-1557, October 1987. Publisher: Optica Publishing Group.
- [4] B. Yurke, M. L. Roukes, R. Movshovich, and A. N. Pargellis. A low-noise series-array Josephson junction parametric amplifier. *Applied Physics Letters*, 69(20):3078–3080, November 1996.
- [5] M. A. Castellanos-Beltran and K. W. Lehnert. Widely tunable parametric amplifier based on a superconducting quantum interference device array resonator. *Applied Physics Letters*, 91(8):083509, August 2007.
- [6] M. A. Castellanos-Beltran, K. D. Irwin, G. C. Hilton, L. R. Vale, and K. W. Lehnert. Amplification and squeezing of quantum noise with a tunable Josephson metamaterial. *Nature Physics*, 4(12):929–931, December 2008.
- [7] F. Mallet. Quantum State Tomography of an Itinerant Squeezed Microwave Field. *Physical Review Letters*, 106(22), 2011.
- [8] M. Malnou, D.A. Palken, Leila R. Vale, Gene C. Hilton, and K.W. Lehnert. Optimal Operation of a Josephson Parametric Amplifier for Vacuum Squeezing. *Physical Review Applied*, 9(4):044023, April 2018.
- [9] Jose Aumentado. Superconducting Parametric Amplifiers: The State of the Art in Josephson Parametric Amplifiers. *IEEE Microwave Magazine*, 21(8):45–59, August 2020.
- [10] Jie-Qiao Liao and C. K. Law. Parametric generation of quadrature squeezing of mirrors in cavity optomechanics. *Physical Review A*, 83(3):033820, March 2011.
- [11] Olivier Pfister, Sheng Feng, Gregory Jennings, Raphael Pooser, and Daruo Xie. Multipartite continuous-variable entanglement from concurrent nonlinearities. *Physical Review A*, 70(2):020302, August 2004.
- [12] C. Eichler. Observation of Two-Mode Squeezing in the Microwave Frequency Domain. *Physical Review Letters*, 107(11), 2011.
- [13] Gustav Andersson. Squeezing and Multimode Entanglement of Surface Acoustic Wave Phonons. *PRX Quantum*, 3(1), 2022.
- [14] Martina Esposito, Arpit Ranadive, Luca Planat, Sébastien Leger, Dorian Fraudet, Vincent Jouanny,

Olivier Buisson, Wiebke Guichard, Cécile Naud, José Aumentado, Florent Lecocq, and Nicolas Roch. Observation of Two-Mode Squeezing in a Traveling Wave Parametric Amplifier. *Physical Review Letters*, 128(15):153603, April 2022.

[15] Shan W. Jolin, Gustav Andersson, J.C. Rivera Hernández, Ingrid Strandberg, Fernando Quijandría, José Aumentado, Riccardo Borgani, Mats O. Tholén, and David B. Haviland. Multipartite Entanglement in a Microwave Frequency Comb. *Physical Review Letters*, 130(12):120601, March 2023.

[16] Kirill Viktorovich Petrovnikin, Michael Romanovich Perelshtain, Tero Korkalainen, Visa Vesterinen, Ilari Lilja, Gheorghe Sorin Paraoanu, and Pertti Juhani Hakonen. Generation and Structuring of Multipartite Entanglement in a Josephson Parametric System. *Advanced Quantum Technologies*, 6(1):2200031, 2023.

[17] Fabio Lingua, J.C. Rivera Hernández, Michele Cortinovis, and David B. Haviland. Continuous-Variable Square-Ladder Cluster States in a Microwave Frequency Comb. *Physical Review Letters*, 134(18):183602, May 2025. Publisher: American Physical Society.

[18] Giulio Cerullo and Sandro De Silvestri. Ultrafast optical parametric amplifiers. *Review of Scientific Instruments*, 74(1):1–18, January 2003.

[19] Shota Yokoyama, Ryuji Ukai, Seiji C. Armstrong, Chanond Sornphiphatphong, Toshiyuki Kaji, Shigenari Suzuki, Jun-ichi Yoshikawa, Hidehiro Yonezawa, Nicolas C. Menicucci, and Akira Furusawa. Ultra-large-scale continuous-variable cluster states multiplexed in the time domain. *Nature Photonics*, 7(12):982–986, December 2013.

[20] Moran Chen, Nicolas C. Menicucci, and Olivier Pfister. Experimental Realization of Multipartite Entanglement of 60 Modes of a Quantum Optical Frequency Comb. *Physical Review Letters*, 112(12):120505, March 2014.

[21] C. W. Gardiner and M. J. Collett. Input and output in damped quantum systems: Quantum stochastic differential equations and the master equation. *Physical Review A*, 31(6):3761–3774, June 1985. Publisher: American Physical Society.

[22] Ofer Naaman and José Aumentado. Synthesis of Parametrically Coupled Networks. *PRX Quantum*, 3(2):020201, May 2022. Publisher: American Physical Society.

[23] B. R. Mollow. Quantum Theory of Parametric Amplification. I. *Physical Review*, 160(5):1076–1096, 1967.

[24] Leonardo Ranzani and José Aumentado. Graph-based analysis of nonreciprocity in coupled-mode systems. *New Journal of Physics*, 17(2):023024, February 2015. Publisher: IOP Publishing.

[25] J. C. Rivera Hernández, Fabio Lingua, Shan W. Jolin, and David B. Haviland. Control of multi-modal scattering in a microwave frequency comb. *APL Quantum*, 1(3):036101, September 2024. arXiv:2402.09068 [quant-ph].

[26] F. Lecocq, L. Ranzani, G.A. Peterson, K. Cicak, R.W. Simmonds, J.D. Teufel, and J. Aumentado. Nonreciprocal Microwave Signal Processing with a Field-Programmable Josephson Amplifier. *Physical Review Applied*, 7(2):024028, February 2017.

[27] Christoph L. Bock, J.C. Rivera Hernández, Fabio Lingua, and David B. Haviland. Nonreciprocal scattering in a microwave frequency comb. *Physical Review Applied*, 24(1):014027, July 2025. Publisher: American Physical Society.

[28] Francesco Arzani, Claude Fabre, and Nicolas Treps. Versatile engineering of multimode squeezed states by optimizing the pump spectral profile in spontaneous parametric down-conversion. *Physical Review A*, 97(3):033808, March 2018. Publisher: American Physical Society.

[29] Jonas Landgraf, Vittorio Peano, and Florian Marquardt. Automated Discovery of Coupled-Mode Setups. *Physical Review X*, 15(2):021038, May 2025. Publisher: American Physical Society.

[30] Peter Namdar, Patrick Folge, Carlos E. Lopetegui, Silia Babel, Benjamin Brecht, Christine Silberhorn, and Valentina Parigi. Spectro-temporally tailored Non-Gaussian Quantum Operations in Thin-Film Waveguides, August 2025. arXiv:2508.04578 [quant-ph].

[31] Christian Weedbrook, Stefano Pirandola, Raúl García-Patrón, Nicolas J. Cerf, Timothy C. Ralph, Jeffrey H. Shapiro, and Seth Lloyd. Gaussian quantum information. *Reviews of Modern Physics*, 84(2):621–669, May 2012. Publisher: American Physical Society.